An Intelligent Nano-positioning Control System Driven by an Ultrasonic Motor

Kuang-Chao Fan[1,#] and Zi-Fa Lai[1]

1 Department of Mechanical Engineering, National Taiwan University, 1, Sec. 4, Roosevelt Rd., Taipei, Taiwan
Corresponding Author / E-mail: fan@ntu.edu.tw, TEL: +886-2-2362-0032, FAX: +886-2-2364-1186

KEYWORDS : Ultrasonic motor, FCMAC, LDGI, Nanopositioning

This paper presents a linear positioning system and its control algorithm design with nano accuracy/resolution. The basic linear stage structure is driven by an ultrasonic motor and its displacement feedback is detected by a LDGI (Laser Diffraction Grating Interferometer), which can achieve nanometer resolution.

Due to the friction driving property of the ultrasonic motor, the driving situation differs in various ranges along the travel. Experiments have been carried out in order to observe and realize the phenomena of the three main driving modes: AC mode (for mm motion), Gate mode (for μm motion), and DC mode (for nm motion). A proposed FCMAC (Fuzzy Cerebella Model Articulation Controller) control algorithm is implemented for manipulating and predicting the velocity variation during the motion of each mode respectively. The PCbased integral positioning system is built up with a NI DAQ Device by a BCB (Borland C^{++} Builder) program to accomplish the purpose of an intelligent nano-positioning control.

Manuscript received: November 14, 2007 / Accepted: April 11, 2008

NOMENCLATURE

d = grating pitch
I_{PDi} = output current of the *i*-th photodetector
v = speed of the grating motion
ω_0 = original angular frequency of the laser source
$\triangle\omega$ = beat frequency of the two orthogonal beams

1. Introduction

In recent years, due to the development of nanotechnologies,[1] piezoelectric transducers (PZT) are often adopted as actuators in precision positioning, but their stroke is limited. Therefore, they are generally combined with an additional long-stroke stage in order to accomplish high-resolution and long-stroke properties.[2] However, accompanied assembly and volumetric errors are generated, and the controlling system becomes more complicated. In this investigation the selected actuator is an ultrasonic motor, which is used in its resonant state to drive in long-stroke and at high-speed, as well as in its bending mode to provide nano motion. Therefore both the long-stroke and the high-resolution requirements of a nano-positioning system are achievable.

In the present research of an ultrasonic motor, the speed is generally high (5 to 250 mm/s),[3,4] as far as the driving circuit is concerned, while the requirements of nano-scale positioning has seldom been studied.[5] Hence, in this paper the driving situations are discussed with respect to each driving mode, especially in the case of a varying friction, in order to achieve a low speed control.

Regarding the displacement feedback, Ishii and Nishimura developed a diffraction grating interferometer[6] to achieve nanometer resolution. Wu et al described a double diffraction linear encoder allowing a higher tolerance with respect to angular errors during the motion.[7] Kimura et al fabricated a surface encoder with dual sine-grids of 10μm pitch using a diamond tool with a piezoelectric driver.[8] In this paper a linear diffraction grating interferometer (LDGI) system is proposed following the concept of common-path and using a fine pitch holographic grating scale to obtain nanometer resolution, and a method to eliminate errors of orthogonal signals in order to enhance the accuracy has also been developed.

2. Components and Principles of the Positioning System

2.1 Ultrasonic motor

The actuator system consists of an ultrasonic motor (model HR4) and a drive amplifier (model AB2) to excite the motor, supplied by the Nanomotion Co. of Israel.[9] These two components are combined to create the piezoelectric effect. This effect converts an electrical field into a mechanical motion. The most important operating components are the 4 piezo ceramic elements. When the exciting voltage is applied across the elements in a precise sequence, the front tip of the piezo elements generate an elliptical motion with a frequency of 39.6 KHz. This elliptical motion subsequently drives the stage by a friction force and thus creates the linear motion of the stage. The operational principle of this ultrasonic motor is shown in Fig. 1 where the tip is deliberately separated from the slide in order to show the form of its elliptical motion.[10]

The AB2 drive provides three main driving modes: AC mode, Gate mode, and DC mode, which cover approximately scales of millimeter, micrometer, and nanometer, respectively. Firstly, the AC

mode creates a continuous resonant frequency drive for the long travel with a moderate speed to a point about forty microns before

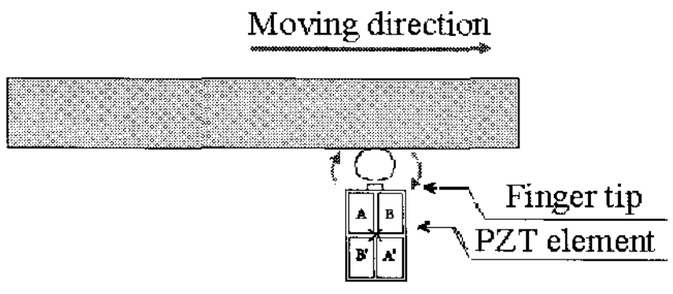

Fig. 1 Motion principle of an ultrasonic motor

reaching the final target position. Secondly, the Gate mode uses periodic on/off pulses of a step size of several microns, in order to drive the stage to a position less than 100nm away from the final target position. Finally, the DC mode makes use of the bending mode principle of the PZT, whereby the driving voltage enables the stage to approach a position closer than 5nm to the final target position. Specifications of the HR4 and AB2 are listed in Table 1 and Table 2.

Table 1 HR4 Specifications

HR4 Specifications	
Maximum Permissable Velocity	250 [mm/sec]
Dynamic Stall Force	15 to 18 [N]
Static Holding Force	14 [N] (reference value)
Maximum Voltage	270 Vrms
Input Wave Form and Frequency	sine wave, 39.6KHz,

Table 2 AB2 Driver Specifications

AB2 Driver Specifications	
Power Input	+24 VDC ±5% (stabilized)
Max. Motor Output	280 Vrms
Input Voltage range	±10V
Input Low Pass Filter	2.7 kHz
DC Mode Output Range	±300nm

2.2 Principle of the LDGI

The LS emits a linearly polarized beam. The P-polarized beam will pass the PBS1 to Q1 (left arm beam) and the S-polarized beam will be reflected on PBS-1 and PBS2 to Q3 (right arm beam). Passing through Q1, the P-polarized left arm beam will change to a right-circularly polarized beam. Similarly, the right arm beam will change to a left-circularly polarized beam after passing Q3. With the emitted angles equal to the grating's ±1 diffraction angles, the input beams will be diffracted back through the same paths to mirrors 1 and 2, respectively. After passing Q1 the left arm will again change to a S-polarized beam and after passing Q3 the right arm will again change to a P-polarized beam. The left arm will be reflected to the Q2-M3-Q2 path and changed to a P-polarized beam, which can pass through PBS1 and PBS2 to Q5, and then changes to a right-circularly polarized beam after passing Q5. Meanwhile, the P-polarized right arm beam will pass through PBS2 and change to a S-polarized after passing through the Q4-M4-Q4 path. Subsequently it is reflected from PBS2 to Q4 and changed to a left-circularly polarized beam after passing Q5. The NPBS divides both the right-circularly and the left-circularly polarized beam into two split beams of equal intensity. These four beams will be divided into 0-90-180-270 degrees by PBS3 and PBS4 (set fast axis to 45 degrees) and interfere with each other. These four orthogonal signals are detected by PD1 to PD4, respectively.

Since the left arm beam is reflected along its -1 diffraction angle and the right arm beam is reflected along its +1 diffraction angle, if the grating is moved laterally with speed v, the frequency shift of each beam due to the Doppler Effect will be:

$$\omega_{+m} = \omega_0 + 2\pi m \frac{v}{d}$$
$$\omega_{-m} = \omega_0 - 2\pi m \frac{v}{d} \quad (1)$$

where, m is the order of diffraction ($m = \pm 1$ here), ω_0 is the original frequency of the laser source, v is the speed of the grating motion, and d is the grating pitch. The frequency difference (beat frequency) of the two interfered beams will be:

$$\Delta\omega = 4\pi m \frac{v}{d} \quad (2)$$

The equations of the optical paths can be derived from the Jones vectors. The intensity of each photo detector can be expressed by:

$$I_{PD1} = A[1 - \sin(2\Delta\omega \cdot t)] \quad (3)$$
$$I_{PD2} = A[1 + \sin(2\Delta\omega \cdot t)] \quad (4)$$
$$I_{PD3} = A[1 + \cos(2\Delta\omega \cdot t)] \quad (5)$$
$$I_{PD4} = A[1 - \cos(2\Delta\omega \cdot t)] \quad (6)$$

Accordingly, by the inspection of the phase variation of the beat frequency signal, the displacement of the grating movement could be measured.

$$\Delta\Phi = \Delta\omega\, t = 4\pi m \frac{v}{d} t = 4\pi m \frac{\Delta x}{d}$$

It can be seen, that when the grating moves by d/2 the beat frequency signal has a phase variation of periodicity (2π). With the holographic grating of 1200 lines/mm, there is an orthogonal signal every 416 nm.

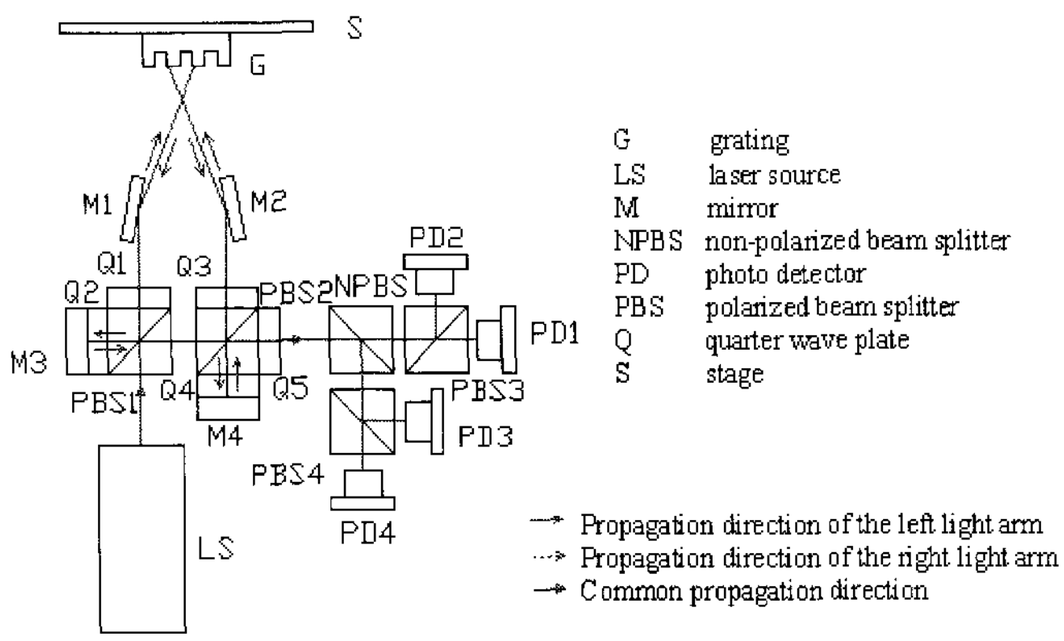

Fig. 2 LDGI optical system design

2.3 LDGI Signal Processing

In classical orthogonal waveforms there are three major error sources. As described by Heydemann,[11] these are:

1. Lack of quadrature (the phase shift between two signals is not exactly $\lambda/4$ or $\pi/2$),
2. unequal gain in the detector channels, and
3. zero offset.

The third error can be corrected by using differential signals, i.e. Eq. (4) minus Eq. (3) and Eq. (5) minus Eq. (6) in order to get the DC corrected two sinusoidal forms. To correct the first error, it is possible to use a vector summation and subtraction operation in order to obtain the exact orthogonal waveforms. The second error should be

corrected by a filtering process using an electronic circuit or by software. The schematic diagram of the signal processing circuit is shown in Figure 3.

After the first two errors have been corrected, the output sinusoidal waves can be reformed to perfect shapes, as shown in Figure 4a. Figure 4b plots its Lissajous diagram. The pulse counting method applies a common up/down counter and the signal subdivision method uses a look-up table (LUT) of tangent values (for the ranges of 0-45, 135-225, 315-360 degrees, respectively) and arc-tangent values (for the other regions). Since one wave cycle corresponds to 416 nm of the grating displacement, we can easily reach a 1 nm resolution after a signal subdivision.

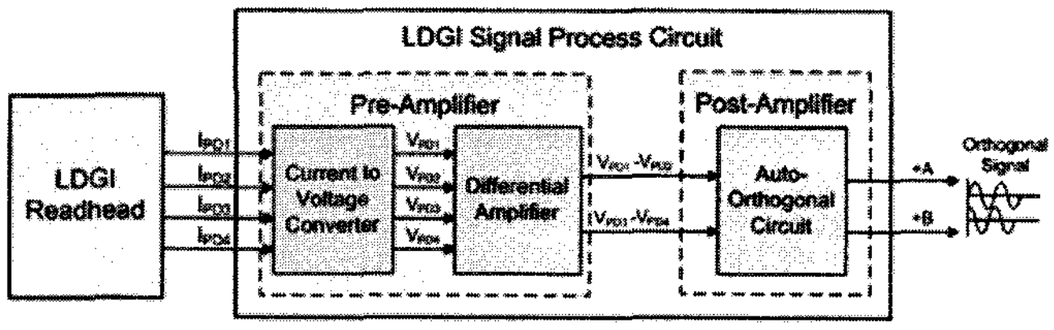

Fig. 3 Schematic diagram of the LDGI signal process

Fig. 4a Corrected waveforms

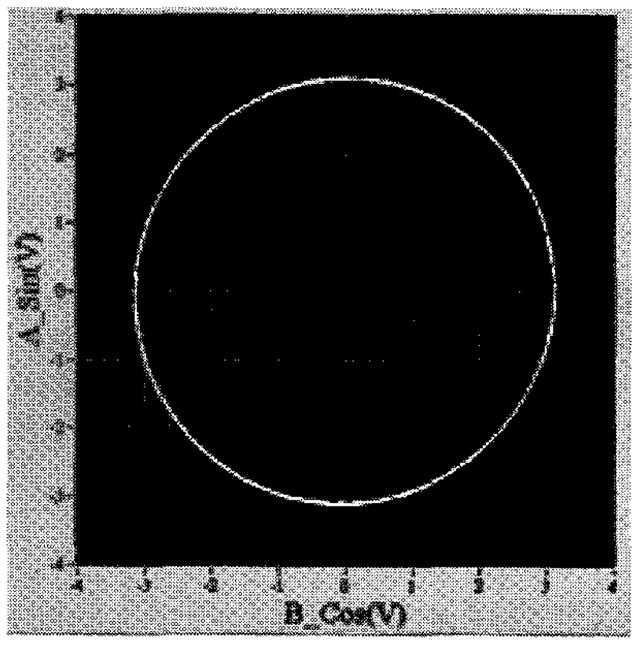

Fig. 4b Lissajous diagram after correction

In a normal nano-positioning stage, the stroke and physical size are small. The LDGI set must be proportionally small. For a compact size design all optics components are selected to be as small as possible. The overall dimension of the developed LDGI is about $50x30x30mm^3$, as is shown in Figure 5.

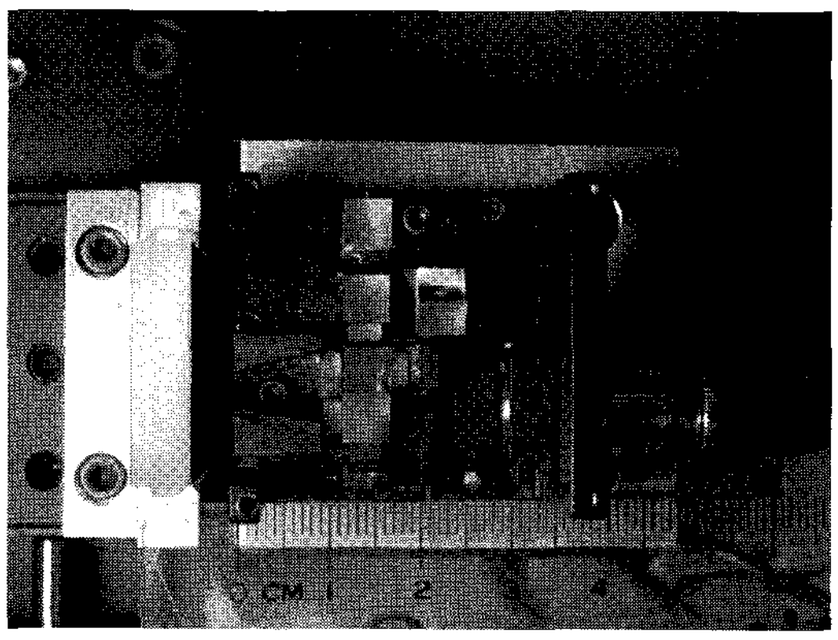

Fig. 5 Photo of the LDGI

2.4 FCMAC Algorithm

The Cerebella Model Articulation Controller (CMAC) was first presented by J. S. Albus in 1975, based on the operation of human cerebella using the properties of generalization and fast learning.[12] The CMAC consist of several layers with various mappings, mapping different input status to specific memory indices of binary weighting values or various basis functions. Due to these advantages of a CMAC, the algorithm can be used to approximate a wide variety of nonlinear functions for a real time robot manipulator control. In addition, the simple structure of a CMAC allows an easy hardware implementation.

The generalized properties of a CMAC can help to reduce the memory allocation in the algorithm. Nevertheless, the required size is still enormous. Many algorithms are implemented on a CMAC [13]. On demand of higher resolution and lower memory consumption, the most common methods are the Differential CMAC (DCMAC) and the Fuzzy CMAC (FCMAC). The DCMAC provides a differential property in order to enhance the resolution, while the FCMAC utilizes fuzzy properties on weight spreading to strengthen the operation. We chose a FCMAC to replace the binary weighting, as is shown in Fig. 6. In this framework, S represents the input space with variables S_1 and S_2, A is the association memory corresponding to S, B is composed of n-th order B-Splines with four basis functions in each group, W denotes the physical space and Y indicates the output space.

Compared to a Neural Network,[14, 15] the advantage of a CMAC is the excellent learning convergence paired with a simple structure, which abandons several node and layer adjustment. Its disadvantage, however, is the necessary memory. With a higher dimension the memory requirement increases enormously. Compared to a CMAC, a FCMAC uses the fuzzy concept so that the memory unit, which corresponds to the input state, can be adjusted by the weighting factors through a learning process. It requires less memory but obtains a higher resolution. A FCMAC possesses many features, such as: good local connectivity; easy to learn complex and nonlinear functions without knowing its transfer function or mathematical model; less memory even in a multi-dimensional space; adjustable weights only for the related memory unit, instead for the whole memory as needed by a neural network; simple framework that can easily be realized by a hardware design. This is the reason why we adopted this controller.

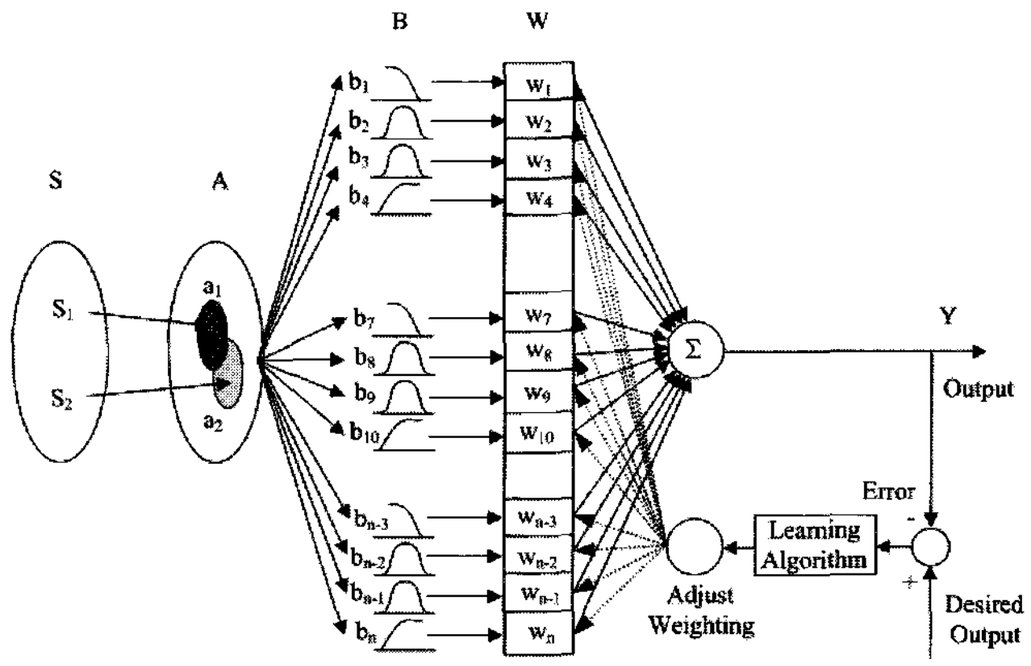

Fig. 6 The diagram of a FCMAC control algorithm

2.5 System Integration

The positioning control system includes an ultrasonic HR4 motor with AB2 drive to move the stage, a LDGI displacement sensor to feed back the current position, and a PC with a FCMAC controller. Fig. 7 shows the block diagram of the system structure. The integration program has been developed with the Borland C^{++} Builder and the DAQ (Data Acquisition)-NI USB 6016 of National Instrument Co. is used to interface signals to a PC. This system was applied to drive a co-planar XY stage[16] developed for a 3D Micro-CMM[10], as shown in Fig. 8.

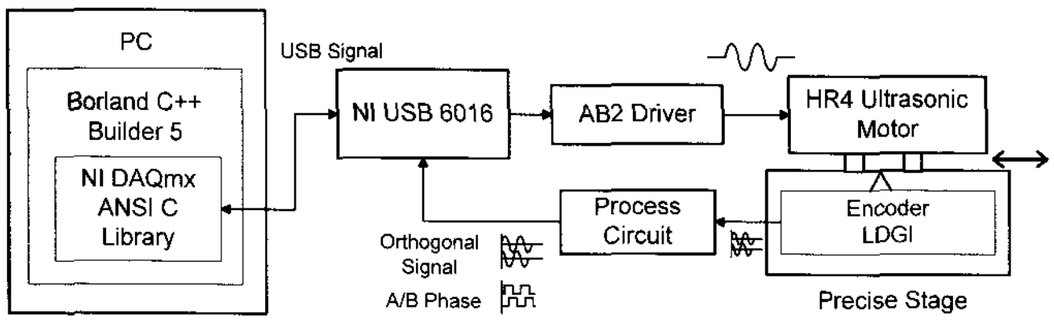

Fig. 7 Block diagram of the control loop

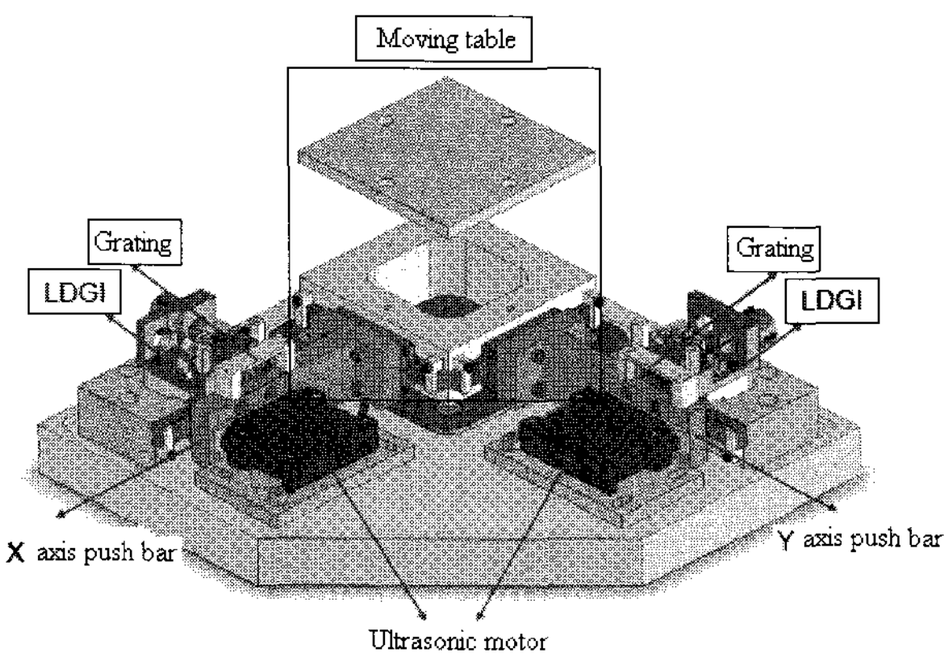

Fig. 8 The Co-planar XY stage

3. Characteristics of Driving Modes and Control Algorithm Design

Since this stage is designed for the particular use in a micro-CMM, the motion is usually in low speed. As indicated in Sec. 2.1, the AB2 driver allows three types of driving modes. Each mode should be tested in order to know its characteristics. Firstly, the AC mode is a continuous drive used in resonance frequency and it is important to control the speed. However, the driving speed variation was extremely large as is shown in Fig. 9, which indicates that the damping is low and hardly allows to estimating parameters such as rise time, settling time, etc. It also reflects the fact, that the vibration of an ultrasonic motor will affect the smoothness of the stage motion. A robust control strategy should be implemented in this case. An initial test with a traditional PID controller did not work well, because the system damping is extremely low. A FCMAC was used to learn two parameters: the driving voltage and the speed variation. With a suitable learning and adjustment of the weights, the AC mode can be controlled under stable conditions. In this AC mode, the input variable is the commanded voltage, which is proportional to the speed of motion, and the output variable is the displacement, which will determine the instantaneous speed and fed back to the FCMAC loop.

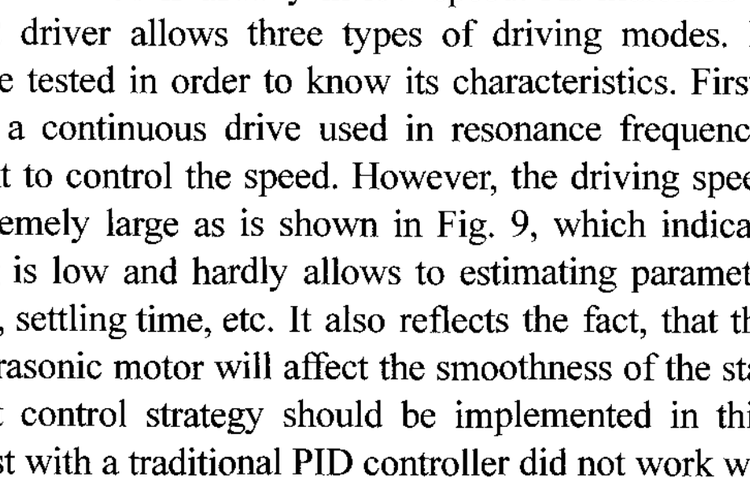

Fig. 9 Speed variation while driving in AC mode

Secondly, the Gate mode is a resonant driving with periodic on/off pulses for the stage moving of less than 10μm. Thus the response of step size with respect to the imposed voltage is of interest. The time necessary for each step is approximately 500 ms yielding a longer target approaching time. An initial test using a gradually decreasing voltage from 1.8 V down to 0.4 V with an increment of 0.5 V was carried out. The step sizes were found to be uneven. To overcome this problem, an alternate voltage input was studied using a FCMAC algorithm. The two input parameters are the desired step and the current friction index in order to get a suitable input voltage. The friction index is obtained from the velocity variation of the previous step and the resulting step. By summation and filtering operations at each time an adequate estimation is yielded and this measure reduced the input variables from 3 to 2, resulting in a smaller memory size and an enhanced efficiency. The FCMAC algorithm could help to generate an adequate index at each input status and, accordingly, adjust the result at each time of driving. In the Gate mode, the input variables are the commanded voltage, which is proportional to the step size, and the pulse width, which controls the speed of motion.

Finally, the DC mode provides a proportional step size to the input voltage with a nanometer motion to the target position. As this mode is critical for the goal of a nano-positioning, the relationship between the input voltage and the output displacement must be investigated. With continuous forward and backward motion commands using the voltage sequence 0→10→-10→0, an obvious hysteresis effect could be observed. Meanwhile, at different stage positions the frictions are different due to the uneven roughness of the machined surface, which will affect the actual displacement, as is shown in Fig. 10. A higher friction results in less displacement. To this effect, Henmi[17] proposed an open-loop method with various experiments to find appropriate control value. Since the motion in DC mode is always one-way to the target point, repeated forward motions by the same voltage command were tested. The results shown in Fig. 11 demonstrate a similar trend at different friction conditions of forward motions only. Based on this characteristic curves the control command will be always a forward motion with different voltages at different moving steps.

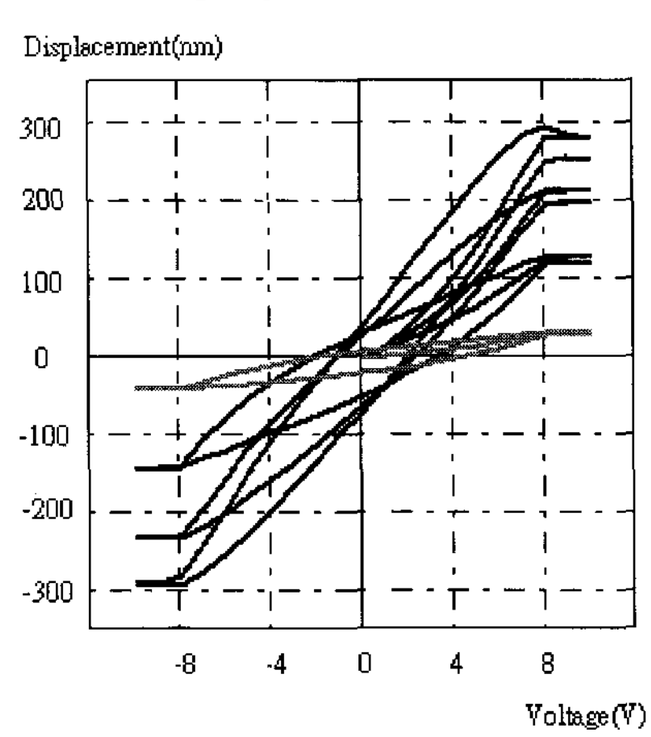

Fig. 10 Displacement changes due to the hysteresis effect of the PZT and the friction effect in DC mode

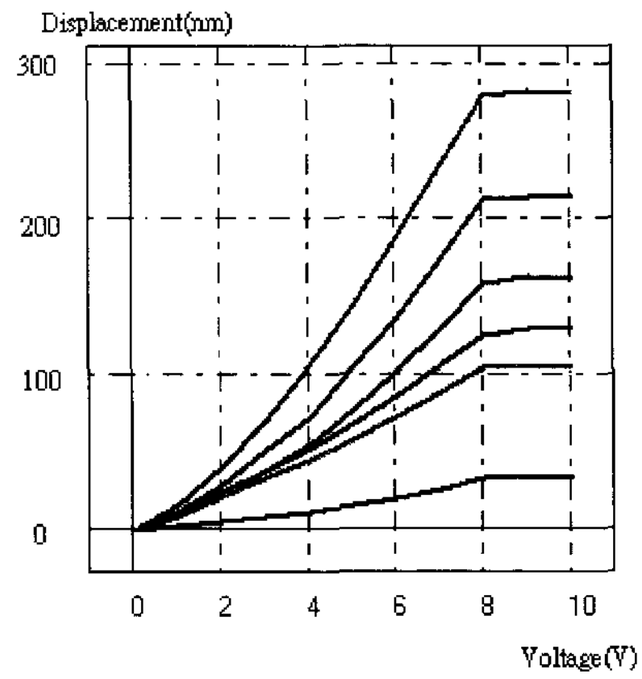

Fig. 11 Repeated forward motions in DC mode under different friction conditions

At the very last step in DC mode the stage will stop in the closest vicinity of the target point. This will determine the positioning accuracy of the stage. In order to realize the fine motion performance, experimental tests were conducted at different voltage levels with the same voltage range of 2 V. Fig. 12 shows a quite consistent linear motion of all curves. This implies that the fine nano-step motion can be controlled by a voltage change and the linear prediction method can be applied in the controller design. This means, that the input voltage is proportional to the displacement. Although the local friction could be varied, which yields different slopes, the friction coefficient could be assumed to be constant within a 100 nm range. Therefore, the incremental voltage can be interpolated linearly, based on the calculated slope.

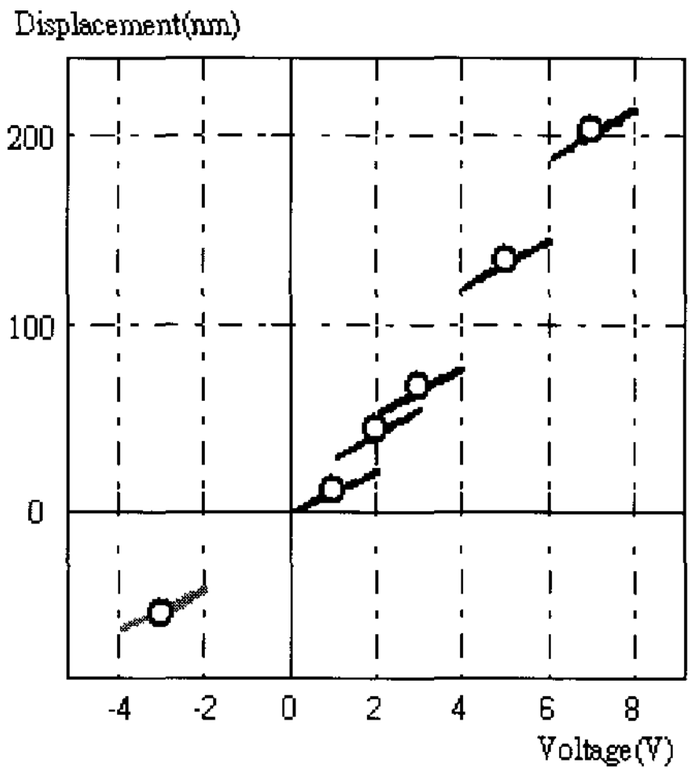

Fig. 12 Linearity of the nano motion in DC mode

After realizing the characteristics of each mode and its corresponding control strategy, the architecture for the whole control algorithm could be determined, as illustrated in Fig. 13, where the AC and the Gate modes together employ the FCMAC control, and the DC mode uses a feed-forward and line prediction method.

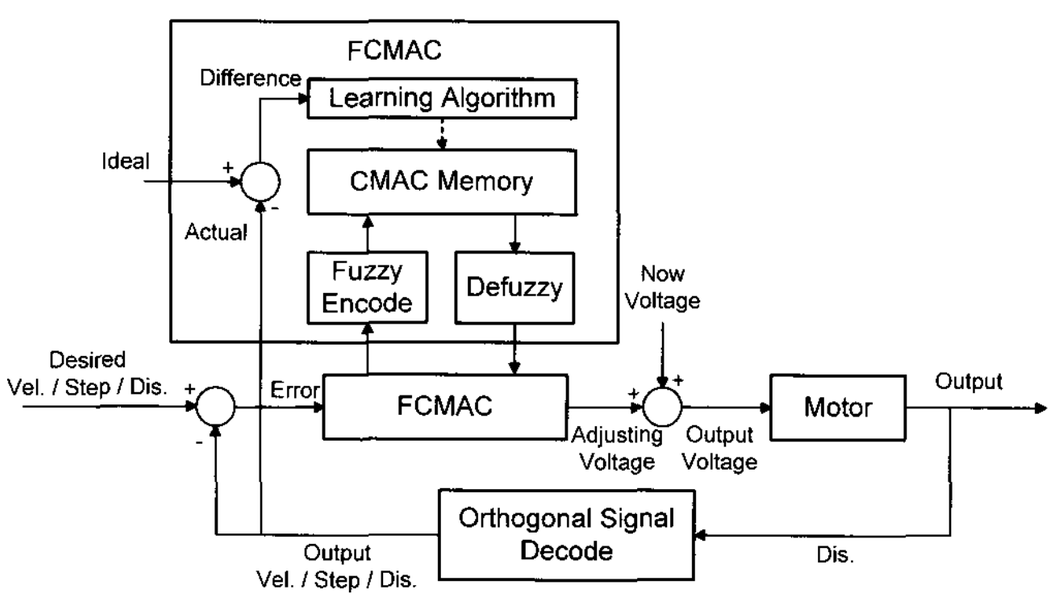

Fig. 13 The system control diagram

4. Experimental Tests

For a long stroke and nano-positioning of a linear stage, three motion modes should be employed. First of all, the long stroke with speed control is conducted by the AC mode. Fig. 14(a) shows the result of speed vs. time, and Fig. 14(b) shows the corresponding voltage change. The speed was well under control at 2 mm/s. There is a slight variation in the voltage change. This is due to the uneven friction effect along the travel. Changing the input voltage keeps the required speed. In many situations the speed is well controlled, hence we can conclude the speed control with the FCMAC learning algorithm is suitable and robust.

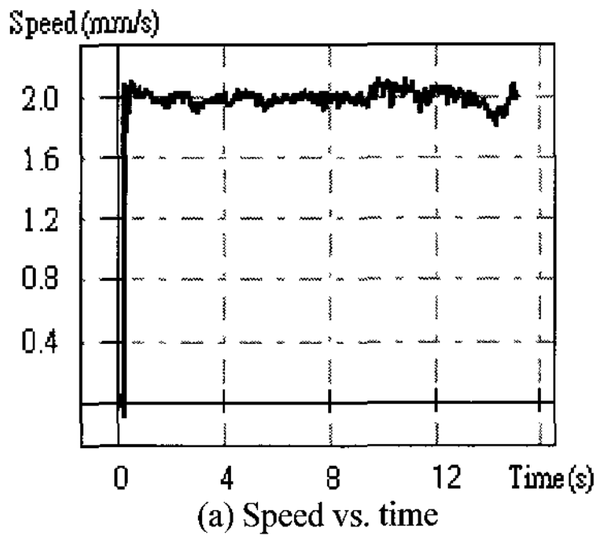

(a) Speed vs. time

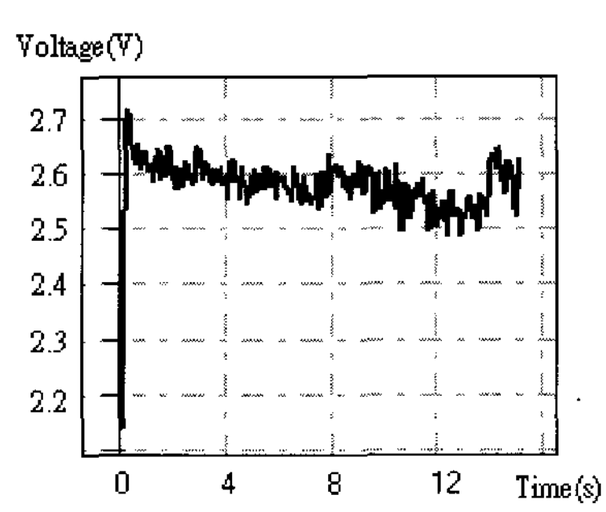

(b) Voltage vs. time

Fig. 14 Long stroke motion in AC mode

Gate and DC modes were subsequently applied for low and fine motions in sequence. Fig. 15(a) shows the results of a 10 μm positioning, where the Gate mode used 3 steps. The first one was the testing step and following two were predicted steps according to the friction status. The Gate mode could move the stage to a position 100 nm before the target position. The DC mode changed the voltage 5 times to arrive to the target position. Fig. 15(b) shows the voltage changes during the motion.

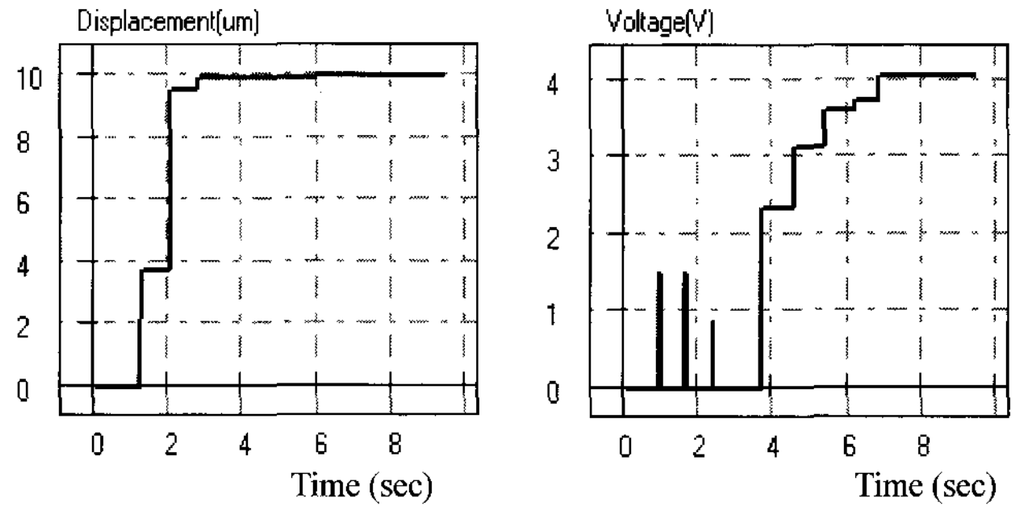

(a) Displacement vs. time (b) Voltage vs. time

Fig. 15 Combination of Gate mode and DC mode motion

Another experiment to check the positioning ability at nano-scale was carried out by a 10 nm step-motion. Fig. 16 shows the result for a 100 nm forward and backward motion. The error is about ±3 nm. This proves that the DC mode is adequate for a nano-positioning control.

5. Discussion

The goal of our research was to develop a new XY nano-position stage (Fig. 8) for a micro-CMM[10]. The workpieces to be measured are all of sizes of millimeters. Therefore, the actual required stage motion is always in the millimeter range. The AC mode provides only a stage motion with low speed to the pre-hit distance of the probe, which is fixed on the Z-axis. The Gate and DC mode motions subsequently move the workpiece at even lower speed to touch the probe, and send the trigger signal to lock the LDGI readings. In this micro-CMM system, the positioning control will be more important than the speed control and the speed variation will cause the 2nd Heydemann error (varied signal amplitudes). This is why our investigation focuses on the speed variation control algorithm of the AC mode. The AC

motion with 2 mm/s is the speed level that we found to be most suitable for our system. If we measure a workpiece of 3 mm length, for example, the AC mode will take only 1.5 seconds.

The hybrid mode motion, combining Gate and DC modes, takes about 7 seconds to reach the target position with a positioning error of ±3 nm, for a stroke of 10 μm (see Fig. 15). In a practical micro-CMM application, the AC mode can cover a longer travel and leaves a stroke of a length of only a few grating pitches for the Gate and DC modes, for instance 2 μm. Thus the remaining controlling time can be reduced. In order to get a very accurate measurement result in the order of nanometers, a measuring time of several seconds is acceptable. This is a trade-off between time and accuracy.

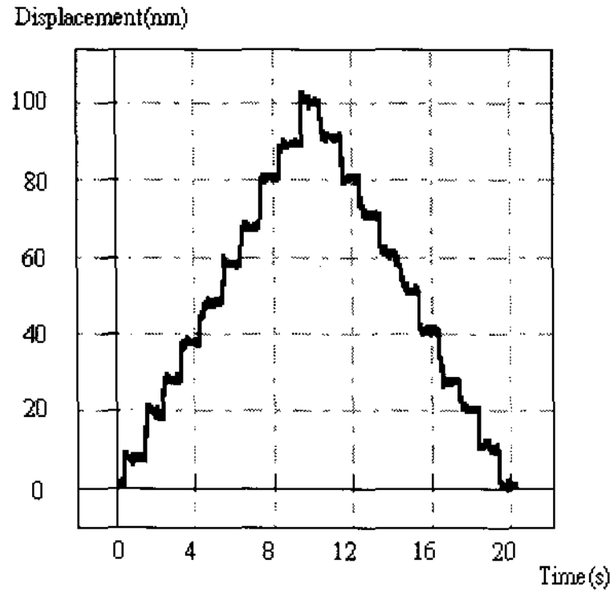

Fig. 16 Step response of the DC mode motion

6. Conclusions

This research proposes the components, the system and the control strategy to establish a long stroke and nano-positioning linear stage motion. An ultrasonic motor is used as the actuator and a LDGI has been developed for the displacement feedback. Three motion modes are studied in order to understand each of the characteristic curves, and the corresponding control algorithms are proposed to obtain the best motion condition. The AC mode can conduct a fast and long stroke motion with the speed controlled by an FCMAC control algorithm. The Gate mode with the FCMAC algorithm can carry the stage to the vicinity of the target point. The DC mode subsequently drives the stage to the final target point with nanometer accuracy.

Compared to other two-stage linear systems, our developed one-stage system is simple in structure, easy to control and of low total cost.

ACKNOWLEDGEMENT

Parts of this research were sponsored by the National Science Council of ROC on the development of a nano-positioning stage.

REFERENCES

1. Mckeown, P., "Nanotechnology-Special article," Proc. of the Nano-metrology in Precision Engineering, pp. 5-55, 1998.

2. Juluri, B.K., Lin, W. and Lim, L., "Long range and high axial load capacity nanopositioner using single piezoelectric actuator and translating supports," International Journal of Precision Engineering and Manufacturing, Vol. 8, No. 4, pp. 3-9, 2007.

3. Peng, Y. F., Wai, R. J. and Lin, C. M., "Implementation of LLCC-Resonant Driving Circuit and Adaptive CMAC Neural Network Control for Linear Piezoelectric Ceramic Motor," IEEE Trans. on Industrial Electronics, Vol. 51, No. 1, pp. 35-48, 2004.

4. Shyu, K. K. and Chang, C. Y., "Anti-windup Controller Design for Piezoelectric Ceramic Linear Ultrasonic Motor Drive," IECON Proceedings (Industrial Electronics Conference), Vol. 1, pp. 341-346, 2003.

5. Fan, K.C., Cheng, F. and Chen, Y.J., "Nanopositioning control on a commercial linear stage by software error compensation," Nanotechnology and Precision Engineering of China (ISSN 1672-6030), Vol. 4, No. 1, pp. 1-9, 2006.

6. Nishimura, T., Kubota, Y., Ishii, S., Ishizuka and Tsukiji S. M., "Encoder Incorporating a Displaceable Diffraction Grating," U. S. Patent No. 5038032, 1991.

7. Wu, C. C., Chen, Y. C., Lee, C. K., Hsieh, C. T., Wu, W. J. and Lu, S. S., "Design Verifications of a Linear Laser encoder with High Head-to-scale Tolerance," Proceedings of SPIE: The International Society for Optical Engineering, Vol. 3779, pp. 73-82, 1999.

8. Kimura, A., Gao, W. and Kiyono, S., "Design and Construction of a Surface Encoder with Dual Sine-Grids," International Journal of Precision Engineering and Manufacturing, Vol. 8, No. 2, pp. 20-25, 2007.

9. Nanomotion Ltd. "AB2 driver user manual," P/N: AB02458000A, www.nanomotion.com, 2003.

10. Fan, K. C., Fei. Y. T., Yu, X. F., Chen, Y. J., Wang, W. L., Chen, F. and Liu, Y. S., "Development of a Low Cost Micro-CMM for 3D Micro/nano Measurements," Measurement Science & Technology, Vol. 17, Issue 3, pp. 524-532, 2006.

11. Heydemann, P. L. M., "Determination and Correction of Quadrature Fringe Measurement Errors in Interferometers," Applied Opt., Vol. 20, No. 19, pp. 3382-3384, 1981.

12. Albus, J. S., "A New Approach to Manipulator Control: The Cerebellar Model Articulation Controller (CMAC)," Journal of Dynamic System, Measurement and Control, Transaction of ASME, Vol. 97, Series G, No. 3, pp. 220-227, 1975.

13. Kwan, C. M., Xu, H., Lewis, F. L., Haynes, L. and Pryor, J. D., "Robust Spacecraft Attitude Control using Fuzzy CMAC," IEEE International Symposium on Intelligent Control, pp. 43-48, 1996.

14. Yin, S.N., Hwang, Y.T. and Yi, W., "Applying an artificial neural network to the control system for electrochemical gear-tooth profile modifications," International Journal of Precision Engineering and Manufacturing, Vol.8, No.4, pp. 33-37, 2007.

15. Lin, F.J., Wai, R.J. and Chen, M.P., "Wavelet neural network control for linear ultrasonic motor drive via adaptive sliding-mode technique," IEEE TRANSACTIONS on Ultrasonics, Ferroelectrics, and Frequency Control, Vol. 50: No. 6, pp. 686-698, 2003.

16. Fan, K. C., Liu, C. L., Wu, P. T., Chen Y. C. and Wang, W. L., "The structure design of a micro-CMM with Abbé principle," Proc. of the 35th International Matador Conf., pp. 297-300, 2007.

17. Henmi, N. and Tanaka, M., "An open-loop method for point-to-point positioning of a piezoelectric actuator," International Journal of Precision Engineering and Manufacturing, Vol. 8, No. 2, pp. 9-13, 2007.